Frequency shifts in noble-gas comagnetometers

W. A. Terrano,[1,*] J. Meinel,[1,†] N. Sachdeva,[2] T. E. Chupp,[2] S. Degenkolb,[3] P. Fierlinger,[1] F. Kuchler,[4] and J. T. Singh[5]

[1] *Physikdepartment, Technische Universität München, Boltzmannstrasse 2 / EXC, 85748 Garching, Germany*
[2] *Department of Physics, University of Michigan, Ann Arbor, Michigan 48109, USA*
[3] *Institut Laue-Langevin, CS 20156, F-38042 Grenoble Cedex 9, France*
[4] *TRIUMF, Vancouver, British Columbia, Canada V6R 2Z9*
[5] *National Superconducting Cyclotron Laboratory and Department of Physics and Astronomy, Michigan State University, East Lansing, Michigan 48824, USA*

(Received 29 July 2018; revised manuscript received 9 February 2019; published 3 July 2019)

Polarized nuclei are a powerful tool in nuclear-spin studies and in the search for physics beyond the standard model. Systems which compare two nuclear species have thus far been limited by anomalous yet reproducible frequency variations of unknown origin. We studied the self-interactions in a ^{3}He-^{129}Xe system by independently addressing, controlling, and measuring the influence of each component of the nuclear-spin polarization. Our results directly rule out prior explanations of the shifts and demonstrate experimentally that they can be explained by species-dependent self-interactions. We also report a gas-phase frequency shift induced by ^{129}Xe on ^{3}He.

DOI: 10.1103/PhysRevA.100.012502

I. INTRODUCTION

Noble-gas magnetic resonance techniques [1] find applications in medical imaging [2,3], atomic gyroscopes [4], and tests of physics beyond the standard model [5–8]. The most precise applications are often limited by unaccounted for frequency variations. Understanding the physical origin of these variations directly impacts the future of ^{3}He-^{129}Xe probes for Lorentz violation [9–11], the ^{129}Xe electric dipole moment [12], fifth forces [13], and direct detection of axionic and "fuzzy" dark matter [14]. More generally, some types of precision atomic gyroscopes [15], magnetometers [16], and, possibly, quantum memory technologies [17] will need to account for these effects.

Fully exploiting the sensitivity of these techniques requires an understanding of the self-interactions of the gases, as was made clear by a recent test of Lorentz violation using a cohabitating ^{3}He-^{129}Xe magnetometer [11]. That work set a limit on the preferred reference frames in the nuclear sector that remains the tightest by a factor of four. Their limit of 3.6 nHz on sidereal frequency variations was extracted on top of μHz-level anomalous frequency variations. The explanation for these variations in terms of self-interactions due to the transverse gas magnetization was controversial [18,19] and, as demonstrated here, incorrect. We present a technique to dynamically control of each component of the nuclear magnetization and use it to measure the self-interactions of the ^{3}He-^{129}Xe system. Our results rule out transverse magnetization as the dominant source of the frequency variations and show that self-interactions coupling to the longitudinal magnetization can explain the observed variations.

A comagnetometer experiment corrects for the effects of magnetic field variations by comparing the frequencies or phases of two species, for instance by defining the corrected frequency

$$\widetilde{\omega}_k(t) = \omega_k(t) - \omega_m(t)\gamma_k/\gamma_m, \tag{1}$$

where k and m label the two distinct spin species and γ_k, γ_m are their gyromagnetic ratios. The search for new physics looks for variations in $\widetilde{\omega}(t)$ that correlate with an experimental parameter.

Several recent experiments reported anomalous variations in $\widetilde{\omega}(t)$ on timescales of several-hundred seconds [10–13,20]. We observed similar variations in our apparatus, with Fig. 1 showing a representative example.

To investigate the source of comagnetometer variations, we directly measured frequency shifts proportional to the transverse-rotating ($M^{\mathrm{T}} \propto \sin\theta_{\mathrm{s}}$) and longitudinal-static ($M^{\mathrm{L}} \propto \cos\theta_{\mathrm{s}}$) magnetizations of each species. Here, θ_{s} is the tip angle of the spins relative to the background magnetic field. We characterize the shifts in ω_k in terms of coupling parameters ρ and λ:

$$\omega_k^{\mathrm{T}} = \sum_{j=\mathrm{He,Xe}} \rho_k^j M_j^{\mathrm{T}}, \tag{2a}$$

$$\omega_k^{\mathrm{L}} = \sum_{j=\mathrm{He,Xe}} \lambda_k^j M_j^{\mathrm{L}}, \tag{2b}$$

which can produce time-dependent drifts in the corrected frequency,

$$\widetilde{\omega}_k^{\mathrm{T}}(t) = \widetilde{\rho}^{\,k} M_k^{\mathrm{T}}(0)e^{-t/T_2^{*(k)}} - r_{km}\widetilde{\rho}^{\,m} M_m^{\mathrm{T}}(0)e^{-t/T_2^{*(m)}}, \tag{3}$$

$$\widetilde{\omega}_k^{\mathrm{L}}(t) = \widetilde{\lambda}^k M_k^{\mathrm{L}}(0)e^{-t/T_1^k} - r_{km}\widetilde{\lambda}^m M_m^{\mathrm{L}}(0)e^{-t/T_1^m}, \tag{4}$$

*Present address: Department of Physics, Princeton University, Princeton, New Jersey 08550, USA; wterrano@princeton.edu

†Present address: University of Stuttgart, 3rd Physics Institute, Pfaffenwaldring 57, Stuttgart 70569, Germany; jonas.meinel@pi3.uni-stuttgart.de

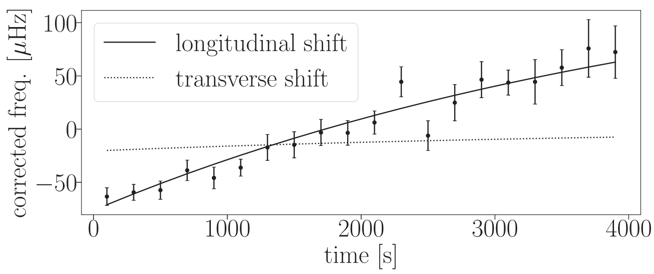

FIG. 1. The corrected frequency $\widetilde{\omega}_{\rm He}(t)/2\pi$ [Eq. (1), offset subtracted] from our data, showing variations similar to those previously reported. The dotted curve indicates the largest shifts due to transverse magnetization that are consistent with the results of this paper. The previously proposed explanation for the variations is excluded. We also measured shifts proportional to longitudinal magnetization. They match the observed variations well (solid curve). See Sec. VI for details of the models used to calculate these curves.

as the gas magnetizations $M^{\rm T}$ and $M^{\rm L}$ decay with phenomenological time constants T_2^* and T_1. Here, $r_{km} = \gamma_k/\gamma_m$, $\widetilde{\lambda}^k = \lambda_k^k - r_{km}\lambda_m^k$, and $\widetilde{\rho}^k = \rho_k^k - r_{km}\rho_m^k$.

Our main findings are as follows: (i) transverse frequency shifts [Eq. (2a)] cannot explain the variations we measured in $\widetilde{\omega}(t)$, contradicting several prior papers [10,11,13]; (ii) longitudinal frequency shifts [Eq. (2b)] are the largest effect and $\lambda_k^k/\gamma^k \neq \lambda_m^k/\gamma^m$ so, crucially, the longitudinal shifts do not cancel in the comagnetometer and can produce slow frequency variations; and (iii) the longitudinal comagnetometer shift is due to resonant effects and direct contact interactions between the noble-gas nuclei rather than magnetic-gradient sampling effects.

II. PARAMETRIZATIONS AND THE THEORY OF INTERNAL FIELDS

A key point of controversy [11,18,19,21,22] has been the magnitude of the internal magnetic fields ($\mathbf{B}_{\rm int}$) in a Rb-free ^{3}He-^{129}Xe cell. Inside a uniformly magnetized sphere, the field experienced by species k is entirely due to contact interactions with species m. This gives $\mathbf{B}_{{\rm int},m} = \frac{2\mu_0}{3}\kappa_{km}\mathbf{M}_k$, where κ parameterizes the overlap between the spin species [23]. This is a scalar interaction and symmetric for $k \leftrightarrow m$. Since the ^{3}He and ^{129}Xe nuclei do not directly overlap, κ_{km} is zero at first order for a ^{3}He-^{129}Xe gas mixture. Contact interactions require higher-order couplings through the electronic spins or a mediator species [24]. Recently, a nonzero $\kappa_{\rm HeXe}$ was measured in a ^{3}He-^{129}Xe comagnetometer with a cohabitating Rb readout [15].

Deviations from a spherical geometry produce long-range dipolar fields that do not average to zero. We parametrize these fields in terms of $B^i_{\rm dip} = \mu_0\Gamma^i M^i$, where i refers to the axis, and Γ^i are dimensionless factors that depend on the geometry of the cell.

Internal fields from the precessing nuclei can apply Ramsey-Bloch-Siegert shifts to the other nuclei [10], which is the basis for previous explanations that claimed that the transverse magnetization was the origin of the frequency variations.

The relaxation-free Bloch equations $d\mathbf{M}_k/dt = \gamma_k\mathbf{M}_k \times \mathbf{B}_{\rm int}$ taken together with $\mathbf{B}_{\rm int} = B^i_{\rm dip} = \mu_0\Gamma^i M^i$ show a resonant shift due to the longitudinal magnetization ($M^{\rm L}$) in a nonspherical cell. Averaging over a Larmor cycle, the transverse field becomes $B_k^{\rm T} = \mu_0\Gamma^{\rm T}M_k^{\rm T}$, and the transverse magnetization precesses at

$$\omega_k = \mu_0\gamma_k\big[(\Gamma^{\rm L} - \Gamma^{\rm T})M_k^{\rm L} + \Gamma^{\rm L}M_m^{\rm L}\big] \tag{5}$$

relative to the frame rotating at $\gamma_k\mathbf{B}_0$, where $\mathbf{B}_0$ is the external holding field. If the cell is not symmetric about $\mathbf{B}_0$, the variations in Γ add harmonics to Eq. (5). The $\Gamma^{\rm L}$ terms are the net field produced by the longitudinal gas polarizations and cancel in $\widetilde{\omega}$. The $\Gamma^{\rm T}$ term is an additional shift that does not cancel in $\widetilde{\omega}$ as it arises from the resonant torque produced by $B_k^{\rm T}$ on $M_k^{\rm L}$.

Physically, this is easiest to understand in the frame rotating at the Larmor frequency ($\gamma_k\mathbf{B}_0$) of species k. In that frame, species k only experiences the transverse field $B_k^{\rm T}$, which is stationary. The transverse field rotates $M_k^{\rm L}$ into the transverse plane at 90° to $B_k^{\rm T}$ and therefore at 90° to the transverse magnetization that sources $B_k^{\rm T}$. The addition of this transverse component means the total $M_k^{\rm T}$ vector rotates slightly relative to the frame rotating at the Larmor frequency. In contrast, $B_k^{\rm T}$ is not resonant with species m and so $M_m^{\rm L}$ experiences no such effect.

Contact interactions (which produce only heteronuclear shifts) and the resonant effects of Eq. (5) (which produce only homonuclear shifts) both affect the corrected frequency. The combined effects are

$$\begin{aligned}\frac{\omega_k}{\mu_0\gamma_k} &= (\Gamma^{\rm L} - \Gamma^{\rm T})M_k^{\rm L} + (\Gamma^{\rm L} + 2\kappa_{km}/3)M_m^{\rm L},\\ \frac{\widetilde{\omega}_k}{\mu_0\gamma_k} &= \Gamma^{\rm T}\big(M_m^{\rm L} - M_k^{\rm L}\big) + 2\big(\kappa_{km}M_m^{\rm L} - \kappa_{mk}M_k^{\rm L}\big)/3.\end{aligned} \tag{6}$$

Independent control of the precession angle of the two species allows us to separately measure each term in Eq. (6).

III. APPARATUS AND DATA REDUCTION

Figure 2 shows a diagram of the experiment at the FRM-II in Munich. We used two measurement cells: a sealed cell containing Rb and about 0.5 bar of ^{3}He for single-species studies, and a valved cell filled with prepolarized ^{3}He-^{129}Xe-N_2 gas mixture at pressures ranging from 0.3 to 1.6 bars for dual-species studies. The cells were made from 2-mm-thick GE-180 glass. The sealed cell was a blown sphere with a 33-mm-outer-diameter (OD) bulb and a 27-mm-long by 6.2-mm-OD pull-off stem. The valved cell was a 24.8-mm-long, 21.2-mm-OD cylinder bonded to doped-Si wafer endcaps. The valve sealed a small hole in the center of one wafer.

Large ^{3}He and ^{129}Xe polarizations were generated by spin-exchange optical pumping using the 794.8 nm D_1 line of a Rb vapor [25,26]. Polarizing the ^{3}He took several hours at 150 °C, while polarizing the ^{129}Xe took 10 minutes at 110 °C due to its larger spin-exchange rate. We then cooled the cell and adiabatically transported it into the magnetically shielded room where the measurement took place at 28 °C [27].

A 1.6-m-diameter y-axis Helmholtz coil provided a 2.38 μT holding field ($\mathbf{B}_0$). Resonant fields ($\mathbf{B}_1$) applied at

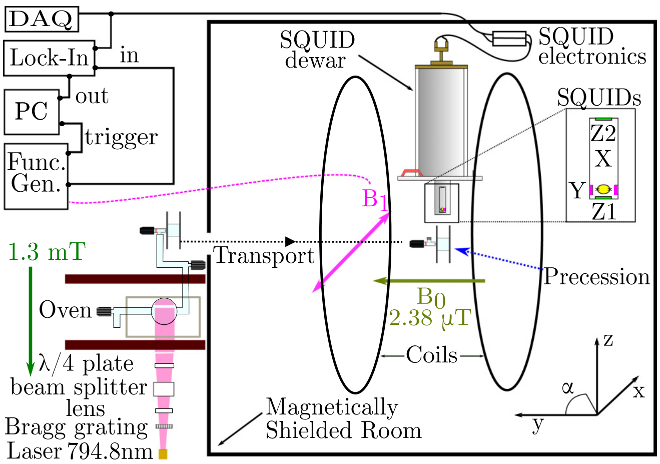

FIG. 2. Diagram of our apparatus. The gas was polarized outside the magnetically shielded room; the spin-precession measurements took place inside the room, directly beneath the superconducting quantum interference device (SQUID) magnetometer system. The combined lock-in, PC, function-generator system allowed us to synchronize our pulses with the precession of the nuclear spins and change the tip angles of the magnetizations during a run.

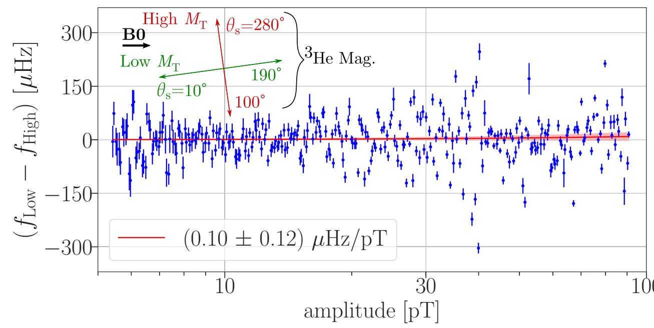

FIG. 3. Difference in ^{3}He frequency at low ($f_{\rm Low}$) and high ($f_{\rm High}$) tip angles θ_s as a function of field from the cell at the SQUID. Each point combines measurements with opposite B_0 projection. The increased scatter near 40 pT amplitude is due to large magnetic field drifts during those measurements, which largely cancel in our final result due to the time-reverse-symmetric tip-angle pattern. Excluding that data entirely also does not change our result: the slope is consistent with zero.

77.2 and 28.0 Hz with a 1.5-m-diameter x-axis Helmholtz coil changed the precession tip angle of the ^{3}He and ^{129}Xe spins, respectively. A set of six SQUID magnetometers directly above the measurement cell monitored the precession of the $M^{\rm T}$ components of the gases.

The SQUID system [28] (lent by PTB-Berlin) contained two SQUIDs oriented along each axis. Subtracting the signals from the two z-axis SQUID magnetometers (separated by 12 cm) formed a gradiometer signal $Z_{\rm grad}$ to suppress background magnetic field fluctuations. The center of the measurement cell was situated variously between 2.8 and 5.8 cm below the lower SQUID.

Changing the tip angle of the precessing spins required $\mathbf{B}_1$ pulses with a particular phase relative to the spins. In order to control for phase drifts between the clock and the spins, we triggered the $\mathbf{B}_1$ pulses from the Z_1 SQUID output.

We recorded the SQUID output signals at a sampling rate of 5 kHz using a 24-bit digitizer (D-TACQ), which was stabilized by an atomic clock (SRS FS725). After downsampling the data to 500 Hz, we divided it into 5-second sections and fitted each section n of $Z_{\rm grad}$ to

$$a_{\rm He}\sin(\omega_{\rm He}t) + b_{\rm He}\cos(\omega_{\rm He}t) + a_{\rm Xe}\sin(\omega_{\rm Xe}t) + b_{\rm Xe}\cos(\omega_{\rm Xe}t) + c_1 t + c_0, \tag{7}$$

where the $a, b, \omega,$ and c were free parameters. Here, $\arctan(a_{\rm He,Xe}/b_{\rm He,Xe}) = \phi^n_{\rm He,Xe}$ gave the instantaneous ^{3}He and ^{129}Xe phases ϕ^n at the start of section m (time t^n). The total phase accumulated at t^n was $\Phi^n_{\rm He,Xe} = \phi^n_{\rm He,Xe} + 2\pi N^n_{\rm He,Xe}$, where $N_{\rm He,Xe}$ counts the number of completed cycles.

To cancel magnetic field fluctuations, we defined adjusted phases. For two species, we used $\widetilde{\Phi}_k(t) = \Phi_k - r_{km}\Phi_m$. For single-species measurements, we defined $\widehat{\Phi}^n_k = \Phi_k(t^n) - \gamma_k \mathcal{G}\int_0^{t^n}[B_y(t) - B_y(0)]dt$, with B_y measured by the y-axis SQUID magnetometers, which coincided with $\mathbf{B}_0$. The scaling factor $\mathcal{G}$ was SQUID and geometry dependent. Fits to $\widetilde{\Phi}_k(t^n)$ or $\widehat{\Phi}_k(t^n)$ gave the corrected frequencies and frequency variations.

IV. FREQUENCY SHIFTS DUE TO TRANSVERSE MAGNETIZATION

The first explanations for the comagnetometer variations ascribed them to Ramsey-Bloch-Siegert shifts from the transverse magnetization of each species on itself [10,11,13]. This explanation predicts a shift in the frequency when measured with different transverse amplitudes. Such a shift is difficult to model, motivating a direct experimental study.

Using the sealed cell– which could achieve very high ^{3}He magnetizations– we applied phase-matched nuclear magnetic resonance (NMR) pulses to move the magnetization between four tip angles: low transverse amplitude (10° and 190°) and high transverse amplitude (100° and 280°), as shown in the Fig. 3 inset. Averaging pairs with opposite B_0 projection cancels shifts from the changes in longitudinal magnetization. Changing the tip angle every 30 seconds kept the background magnetic field generally stable between opposite projections. We reversed the tip-angle sequence every 120 seconds to invert the effects of linear-in-time magnetic field changes.

For every set of four tip angles, we calculated the frequency difference between the high and low tip-angle states and determined the transverse magnetization from the amplitude of the precession signal. As shown in Fig. 3, we saw no evidence that the ^{3}He precession frequency depends on the magnitude of the transverse magnetization. We constrain $\rho^{\rm He}_{\rm He}/2\pi < 6.1$ mHz/(A/m) at the 68% confidence level.

V. FREQUENCY SHIFTS DUE TO LONGITUDINAL MAGNETIZATION

While measuring transverse shifts, we observed and canceled large longitudinal frequency shifts. To further investigate the longitudinal shifts, we applied a $\mathbf{B}_1$ field that produced both transverse and longitudinal magnetizations. A

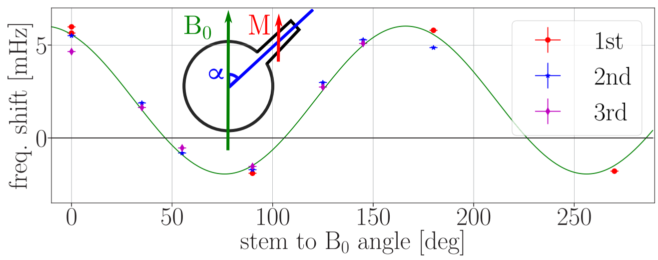

FIG. 4. Change in ^{3}He frequency on inverting the ^{3}He magnetization, as a function of cell orientation. The curve is $(3\cos^2\alpha - 1) \times 2.7$ mHz, with a 0.7 mHz offset, corresponding to the angular dependence of the average field in the cell produced by a ^{3}He dipole (**M**) at the stem. The offset is likely due to α-symmetric asphericities, such as oblateness of the sphere.

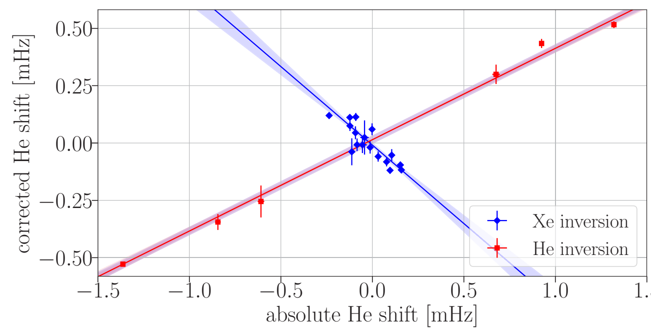

FIG. 5. Change in the absolute ($\omega_{\rm He}$) and corrected ($\widetilde{\omega}_{\rm He}$) ^{3}He frequencies when the longitudinal magnetizations of ^{129}Xe and ^{3}He are inverted (blue diamonds and red squares). Measurements taken in the valved cell; some errors are hidden by the symbols. The slope of the lines measures the shifts in the ratios of interest, with 1-σ error (shaded) from the covariance of the fit to a line. If the comagnetometer correction canceled frequency shifts from longitudinal magnetization [Eq. (2b)], the lines would be horizontal.

train of π pulses then flipped $M^{\rm L}$ and any frequency shifts associated with it.

Figure 4 shows the dependence of the longitudinal shift on cell orientation for the sealed cell. The shift is proportional to $(3A\cos^2\alpha - A)$, where α is the stem-to-B_0 angle and A is the shift amplitude, as is expected for a shift generated by the ^{3}He dipole in the stem. Based on analytical calculations using the measured cell geometry, we estimated that the gas in the stem would produce a net magnetic field of (45 ± 15) pT across the cell, dominated by the field within the stem. The corresponding shift from a static dipole would be $A_{\rm dipole} = (1.5 \pm 0.5)$ mHz. The ^{3}He dipole, however, also has a rotating component, so the second term of Eq. (5) amplifies the frequency shift by a factor of $3/2$ and we predict $A_{\rm model} = (2.25 \pm 0.75)$ mHz. The measured $A_{\rm expt.} = (2.7 \pm 0.1)$ mHz agrees with our geometric estimate of the resonant enhancement.

Longitudinal shifts do not cancel in the corrected frequency, as shown in Fig. 5, so the decay of $M_m^{\rm L}$ causes time variations in $\widetilde{\omega}(t)$. We experimentally measured $\widetilde{\lambda}^{\rm He} = (750 \pm 60)$ mHz/(A/m) for our system and isolated the physical mechanisms responsible for the finite $\widetilde{\lambda}$.

To investigate whether magnetic field gradients explained the nonzero $\widetilde{\lambda}$ [29], we used a small coil that mimicked the gradients of the cell. For a given change in the helium frequency, the corrected frequency shift produced by the coil is 100 times smaller than the shift produced by the nuclear-spin polarization.

To separately measure all of the geometric and contact interactions in Eq. (6), we used each species as both the source and probe of the longitudinal shifts, and changed the geometric effect by changing the cell orientation. We analyzed, in terms of $\Delta^{(m)}\mathcal{R}_k = \Delta^{(m)}(\widetilde{\omega}_k/\omega_k)$, the change in the frequency ratio of species k when the longitudinal polarization of species m is inverted. This ratio is insensitive to changes in polarization and tip angle. Doing this for all four combinations of k and m and at cylinder-axis-to-B_0 angles $\alpha = 0^\circ$ and 90° gave us eight measurements with different sensitivities to κ and Γ.

Table I lists the measured shifts in $\Delta^{(m)}\mathcal{R}_k$ and the κ values extracted from them. All error bars are statistical only

TABLE I. Results from our study of species-specific, longitudinal-magnetization-dependent frequency shifts. *Ratio* gives the species for which we measured $\Delta^{(m)}\mathcal{R}_k = \Delta^m(\widetilde{\omega}/\omega_k)$: the change in the corrected to absolute frequency ratio of species k when the longitudinal magnetization $M_m^{\rm L}$ of species m is flipped. α is the angle of the magnetic field to the cell axis. Model is the theoretical expectation assuming only a scalar κ interaction and resonant geometric effect [Eq. (6)], with Γ_0 defined by $B_{\rm int}^{\rm L}(\alpha) = \mu_0 M^{\rm L}\Gamma_0(3\cos^2\alpha - 1)$ and measured to be $\Gamma_0 = 0.023 \pm 0.002$ from the absolute magnitudes of the homonuclear shifts. Measured value is the value of $\Delta^{(m)}\mathcal{R}_k$ from our full data set. Extracted κ is the κ consistent with $\Delta^{(m)}\mathcal{R}_k$ assuming the model. Fills is the number of separate cell fillings of different pressures that contributed to the measured value, and Shifts is the number of independent measurements of the $\Delta^{(m)}\mathcal{R}_k$ that we made by flipping $M_m^{\rm L}$.

Ratio	α	Model	Measured value	Extracted κ	Fills	Shifts
$\Delta^{(\rm He)}\mathcal{R}_{\rm He}$	0°	$(3\Gamma_0 - 2\kappa_{\rm XeHe})/9\Gamma_0$	0.411 ± 0.008	$\kappa_{\rm XeHe} = -0.0080 \pm 0.0038$	4	34
$\Delta^{(\rm Xe)}\mathcal{R}_{\rm He}$	0°	$(2\kappa_{\rm HeXe} - 3\Gamma_0)/(2\kappa_{\rm HeXe} + 6\Gamma_0)$	-0.639 ± 0.030	$\kappa_{\rm HeXe} = -0.0059 \pm 0.0009$	3	31
$\Delta^{(\rm Xe)}\mathcal{R}_{\rm Xe}$	0°	$(3\Gamma_0 - 2\kappa_{\rm HeXe})/9\Gamma_0$	0.369 ± 0.020	$\kappa_{\rm HeXe} = -0.0036 \pm 0.0039$	3	31
$\Delta^{(\rm He)}\mathcal{R}_{\rm Xe}$	0°	$(2\kappa_{\rm XeHe} - 3\Gamma_0)/(2\kappa_{\rm XeHe} + 6\Gamma_0)$	-0.687 ± 0.021	$\kappa_{\rm XeHe} = -0.0077 \pm 0.0008$	4	34
$\Delta^{(\rm He)}\mathcal{R}_{\rm He}$	90°	$(1.5\Gamma_0 + 2\kappa_{\rm XeHe})/4.5\Gamma_0$	0.140 ± 0.005	$\kappa_{\rm XeHe} = -0.0010 \pm 0.0006$	2	15
$\Delta^{(\rm Xe)}\mathcal{R}_{\rm He}$	90°	$(2\kappa_{\rm HeXe} + 1.5\Gamma_0)/(2\kappa_{\rm HeXe} - 3\Gamma_0)$	-0.143 ± 0.056	$\kappa_{\rm HeXe} = -0.0108 \pm 0.0018$	2	14
$\Delta^{(\rm Xe)}\mathcal{R}_{\rm Xe}$	90°	$(1.5\Gamma_0 + 2\kappa_{\rm HeXe})/4.5\Gamma_0$	0.132 ± 0.046	$\kappa_{\rm HeXe} = -0.0104 \pm 0.0022$	2	14
$\Delta^{(\rm He)}\mathcal{R}_{\rm Xe}$	90°	$(2\kappa_{\rm XeHe} + 1.5\Gamma_0)/(2\kappa_{\rm XeHe} - 3\Gamma_0)$	-0.157 ± 0.008	$\kappa_{\rm XeHe} = -0.0102 \pm 0.0009$	2	15

and determined from the quality of the fits to $\Delta^{(m)}\mathcal{R}_k$. The data set consisted of six separate cell fillings at different pressures, with 16 780 s of data and 130 shift measurements at $\alpha = 0^\circ$ and 8660 s of data and 58 shift measurements at $\alpha = 90^\circ$. To extract κ from our data, we used Eq. (6) along with the geometric relations of a dipole: $\Gamma^{\mathrm{T}} = -\Gamma^{\mathrm{L}}/2$ and $\Gamma^{\mathrm{L}}(90^\circ) = -\Gamma^{\mathrm{L}}(0^\circ)/2$, as a function of cell orientation α. The uncorrected homonuclear shifts, combined with the measured amplitudes, magnetometer-cell distance, and flip angles gave $\Gamma^{\mathrm{L}}(0^\circ) = 0.046 \pm 0.004$.

We measured $\kappa_{\mathrm{HeXe}} = -0.0094 \pm 0.0004$ (weighted mean), while Limes *et al.* recently measured $\kappa_{\mathrm{HeXe}} = -0.011 \pm 0.001$ [15]. A first-principles electronic structure calculation, performed following these initial reports of gas-phase interactions between noble-gas nuclear spins, found similar values along with a prediction for a temperature dependence of κ_{HeXe} [30]. Our data also gives a measurement of the shift induced by ^{129}Xe on ^{3}He: $\kappa_{\mathrm{XeHe}} = -0.0072 \pm 0.0008$ (weighted mean). The comparable sizes of κ_{HeXe} and κ_{XeHe} supports the scalar interaction picture for the frequency shifts.

Our measurements of the internal fields also constrain heteronuclear transverse shifts. With typical values in our comagnetometer system $M^{\mathrm{T}} = 8 \times 10^{-4}$A/m, $\kappa \sim \Gamma \approx -0.01$, and $\Delta = (\omega_{\mathrm{He}} - \omega_{\mathrm{Xe}})/2\pi \sim 50$ Hz, Ramsey-Bloch-Siegert shifts across species would be $(\gamma \mathbf{B}_{\mathrm{int}})^2/2\Delta \sim 4 \times 10^{-10}$ Hz, far below the μHz variations reported in $\widetilde{\omega}(t)$ (Fig. 1 and Refs. [11,19]).

VI. SUMMARY AND CONCLUSIONS

Figure 1 compares our measured $\widetilde{\omega}(t)$ with the maximum possible transverse shift consistent with our measurement $\rho^{\mathrm{He}}_{\mathrm{He}} < 6.1$ mHz/(A/m), taking T_2^* and M^{T} from the precession signal, and showing that transverse shifts are inconsistent with the observed drifts. The longitudinal shifts predicted by our measurements of $\widetilde{\lambda}^{\mathrm{He}} = 750$ mHz/(A/m) are also shown, assuming typical values for our system of $T_1^{\mathrm{Xe}} = 3500$ s, $T_1^{\mathrm{He}} = 5250$ s, and $\theta_s = 89^\circ$; the model matches the data well for a wide range of T_1.

Ruling out the previously published explanations for the drifts [10,11,13,19] required a much better measurement of transverse shifts than has been performed for longitudinal shifts: with $\theta_s \approx 90^\circ$, transverse shifts are significantly enhanced relative to longitudinal shifts. Still, we suggest that the $\widetilde{\omega}(t)$ variation does, in fact, come from longitudinal shifts which do not cancel in the corrected frequency and which decay over the run. We directly measured the magnitude of such a shift, showed it is large enough to explain the drifts, and showed it largely involves two mechanisms: a resonant effect that rotates the longitudinal magnetization into the transverse plane and a direct ^{3}He -^{129}Xe scalar interaction.

These undesirable variations in ^{3}He-^{129}Xe comagnetometers could be reduced by minimizing residual M_{L} and choosing cell geometries where the geometric and scalar internal shifts cancel [15], giving ^{3}He -^{129}Xe comagnetometers a chance to live up to their potential.

ACKNOWLEDGMENTS

The authors thank F. Röhrer and M. Weidenthaler for help with gathering the data. We would also like to thank PTB-Berlin for lending us a SQUID system and lots of help in getting our comagnetometer running. In particular, we thank J. Voigt for helping us keep the SQUID operational, W. Kilian for helping us set up our polarizer, and L. Trahms and S. Knappe-Grüneberg for helpful discussions of magnetometry. We also want to thank E. Babcock for help on the polarizer and the Lurie Nanofabrication Facility for help producing our cells. This work was supported by the DFG Cluster of Excellence "Origin and Structure of the Universe" and Michigan State University. W.A.T. would like to thank the A Von Humboldt Foundation for financial support.

[1] T. E. Chupp, E. R. Oteiza, J. M. Richardson, and T. R. White, Phys. Rev. A **38**, 3998 (1988).

[2] H. E. Möller, X. J. Chen, B. Saam, K. D. Hagspiel, G. A. Johnson, T. A. Altes, E. E. de Lange, and H. Kauczor, Magn. Reson. Med. **47**, 1029 (2002).

[3] *Hyperpolarized Xenon-129 Magnetic Resonance*, edited by T. Meersmann and E. Brunner, New Developments in NMR (The Royal Society of Chemistry, Cambridge, UK, 2015), pp. P001–484.

[4] T. W. Kornack, R. K. Ghosh, and M. V. Romalis, Phys. Rev. Lett. **95**, 230801 (2005).

[5] G. Vasilakis, J. M. Brown, T. W. Kornack, and M. V. Romalis, Phys. Rev. Lett. **103**, 261801 (2009).

[6] J. M. Brown, S. J. Smullin, T. W. Kornack, and M. V. Romalis, Phys. Rev. Lett. **105**, 151604 (2010).

[7] M. Smiciklas, J. M. Brown, L. W. Cheuk, S. J. Smullin, and M. V. Romalis, Phys. Rev. Lett. **107**, 171604 (2011).

[8] J. Lee, A. Almasi, and M. Romalis, Phys. Rev. Lett. **120**, 161801 (2018).

[9] D. Bear, R. E. Stoner, R. L. Walsworth, V. A. Kostelecký, and C. D. Lane, Phys. Rev. Lett. **85**, 5038 (2000).

[10] C. Gemmel, W. Heil, S. Karpuk, K. Lenz, Y. Sobolev, K. Tullney, M. Burghoff, W. Kilian, S. Knappe-Grüneberg, W. Müller, A. Schnabel, F. Seifert, L. Trahms, and U. Schmidt, Phys. Rev. D **82**, 111901(R) (2010).

[11] F. Allmendinger, W. Heil, S. Karpuk, W. Kilian, A. Scharth, U. Schmidt, A. Schnabel, Y. Sobolev, and K. Tullney, Phys. Rev. Lett. **112**, 110801 (2014).

[12] M. A. Rosenberry and T. E. Chupp, Phys. Rev. Lett. **86**, 22 (2001).

[13] K. Tullney, F. Allmendinger, M. Burghoff, W. Heil, S. Karpuk, W. Kilian, S. Knappe-Grüneberg, W. Müller, U. Schmidt, A. Schnabel, F. Seifert, Y. Sobolev, and L. Trahms, Phys. Rev. Lett. **111**, 100801 (2013).

[14] P. W. Graham, D. E. Kaplan, J. Mardon, S. Rajendran, W. A. Terrano, L. Trahms, and T. Wilkason, Phys. Rev. D **97**, 055006 (2018).
[15] M. E. Limes, N. Dural, M. V. Romalis, E. L. Foley, T. W. Kornack, A. Nelson, and L. R. Grisham, arXiv:1805.11578.
[16] H. Koch, G. Bison, Z. D. Grujić, W. Heil, M. Kasprzak, P. Knowles, A. Kraft, A. Pazgalev, A. Schnabel, J. Voigt, and A. Weis, Eur. Phys. J. D **69**, 202 (2015).
[17] O. Katz and O. Firstenberg, Nat. Commun. **9**, 2074 (2018).
[18] M. V. Romalis, D. Sheng, B. Saam, and T. G. Walker, Phys. Rev. Lett. **113**, 188901 (2014).
[19] F. Allmendinger, U. Schmidt, W. Heil, S. Karpuk, A. Scharth, Y. Sobolev, and K. Tullney, Phys. Rev. Lett. **113**, 188902 (2014).
[20] C. Gemmel, W. Heil, S. Karpuk, K. Lenz, C. Ludwig, Y. Sobolev, K. Tullney, M. Burghoff, W. Kilian, S. Knappe-Grüneberg, W. Müller, A. Schnabel, F. Seifert, L. Trahms, and S. Baeßler, Eur. Phys. J. D **57**, 303 (2010).
[21] M. A. Rosenberry, A Precision measurement of the ^{129}Xe electric dipole moment using dual noble gas masers, Ph.D. thesis, University of Michigan, 2000.
[22] E. R. Oteiza, Search for a permanent electric dipole moment in ^{129}Xe using simultaneous ^{3}He magnetometry, Ph.D. thesis, Harvard University, 1992.
[23] S. R. Schaefer, G. D. Cates, T.-R. Chien, D. Gonatas, W. Happer, and T. G. Walker, Phys. Rev. A **39**, 5613 (1989).
[24] A. Vlassenbroek, J. Jeener, and P. Broekaert, J. Magn. Reson., Ser. A **118**, 234 (1996).
[25] T. G. Walker and W. Happer, Rev. Mod. Phys. **69**, 629 (1997).
[26] T. R. Gentile, P. J. Nacher, B. Saam, and T. G. Walker, Rev. Mod. Phys. **89**, 045004 (2017).
[27] F. Kuchler, E. Babcock, M. Burghoff, T. Chupp, S. Degenkolb, I. Fan, P. Fierlinger, F. Gong, E. Kraegeloh, W. Kilian, S. Knappe-Grüneberg, T. Lins, M. Marino, J. Meinel, B. Niessen, N. Sachdeva, Z. Salhi, A. Schnabel, F. Seifert, J. Singh, S. Stuiber, L. Trahms, and J. Voigt, Hyperfine Interact. **237**, 95 (2016).
[28] D. Drung, Physica C: Superconductivity **368**, 134 (2002).
[29] D. Sheng, A. Kabcenell, and M. V. Romalis, Phys. Rev. Lett. **113**, 163002 (2014).
[30] J. Vaara and M. V. Romalis, Phys. Rev. A **99**, 060501(R) (2019).